
Memorandum 008

# The Frequency-Dependent Scattering of Pulsar J1903+0327

Abra Geiger and Michael Lam

2022 August 25

http://nanograv.org/

# The Frequency-Dependent Scattering of Pulsar J1903+0327

Abra Geiger[1,2] and Michael Lam[1,3]

[1]School of Physics and Astronomy, Rochester Institute of Technology, Rochester, NY 14623, USA
[2]Spencerport High School, Spencerport, NY 14559, USA
[3]Laboratory for Multiwavelength Astrophysics, Rochester Institute of Technology, Rochester, NY 14623, USA

August 2022

## 1 Introduction

NANOGrav, the North American Nanohertz Observatory for Gravitational Waves, works to detect gravitational waves through the use of pulsar timing arrays (PTAs). Other subjects of interest which are better understood through the use of PTAs are astronomical phenomena such as the interstellar medium (ISM), General Relativity, and alternate theories of gravity. Pulsars are rotating neutron stars: the collapsed cores of stars gone supernova that spin rapidly via conservation of angular momentum. These rotations are not only rapid but also extremely consistent; their timing consistency rivals that of atomic clocks on Earth. Beams of radio waves are emitted from the poles of pulsars due to magnetic field intensity, and at Earth we receive and measure these periodic radio wave pulses. NANOGrav currently observes an array of approximately 80 millisecond pulsars, which are timed to submicrosecond precision, and submicrosecond deviations from expected times of arrival can indicate the presence of gravitational waves.

## 2 Pulsar Timing and the Interstellar Medium

In order to accurately detect deviations in pulsar timing, an understanding of the intrinsic and extrinsic effects upon pulsar times of arrival (TOAs) is integral. This research focuses on the frequency-dependent effects on TOAs caused by the ISM, specifically scattering. Pulsar J1903+0327, which is analyzed in this research, has a pulsar pulse profile shape consistent with a Gaussian distribution. If our reception of a pulse was perfect, with no error on our end or that caused by the universe, we would expect to see the beam of radio waves emitted from a pulsar first dim as it begins to reach the line of sight, then head-on, and finally followed by a paralleled, dim exiting of the beam – approximately a Gaussian shape. Bright and narrow pulses are ideal for precision TOAs (Cordes et al., 2019). Naturally, however, there is interference from the interstellar medium through which we receive the light, which results in frequency-dependent delays. The ISM is composed of mostly gas,

plasma, dust, and cosmic rays. As a pulsar's beam of radio waves propagates through the ISM, there are three main effects upon it, all of which relate to how electromagnetic waves change speed and direction when they interact with different mediums. First, **dispersion**, which is characterized by the measure of integrated electron density along the line of sight (dispersion measure or DM), causes an overall delay in arrival for all photons at a given frequency. Because of the presence of electrons in the ISM, the pulse is slowed, and this effect on speed is greater at lower frequencies, scaled $\nu^{-2}$. Dispersion is widely accounted for in NANOGrav data sets. Second is **scintillation**. Because electromagnetic waves scatter in different directions in new mediums, an observer may receive varying signal brightness over time. Sometimes the electromagnetic signal is seen to be brighter per the chance that more of the signal has pointed towards the Earth, and other times the signal refracts away and appears dimmer. A similar effect can be observed in stars as they pass through Earth's atmosphere, causing them to vary in brightness or "twinkle". Third is **scattering**. Because electromagnetic waves disperse and change direction in the ISM, multi-path propagation, their paths to the observer are affected. Some paths are elongated while others remain short, and the effect is pulse broadening, or delayed arrival of part of the pulse. The pulse-altering effects of scattering are demonstrated in Figure 1.

# 3 Pulsar J1903+0327

NANOGrav conducts pulsar observations at the 100m Green Bank Telescope (GBT), the Very Large Array (VLA), the Canadian Hydrogen Intensity Mapping Experiment (CHIME) and, prior to its collapse, observed using the William E. Gordon Telescope at the Arecibo Observatory. For our research, we use the NANOGrav 12.5-year data set release collected at the Arecibo Observatory with the Puerto Rican Ultimate Pulsar Processing Instrument (PUPPI) backend for one pulsar, J1903+0327 (Alam et al., 2021). This memorandum analyzes J1903+0327 frequency-dependent scattering. First discovered at Arecibo, J1903+0327 has a pulse period of 2.15 ms, a solar mass companion, and it has even been proposed that J1903+0327 is part of a hierarchical triple system (Champion et al., 2008). This pulsar also has an especially high DM of 297 pc/cm$^3$, the highest DM of any pulsar that NANOGrav observes (Champion et al., 2008). The pulse profile of J1903+0327 very obviously demonstrates the effect of scattering, making it useful in our analysis.

# 4 Modeling

## 4.1 Pulse Shape Convolution

Theoretically, an idealized pulsar pulse can be represented as a Gaussian distribution:

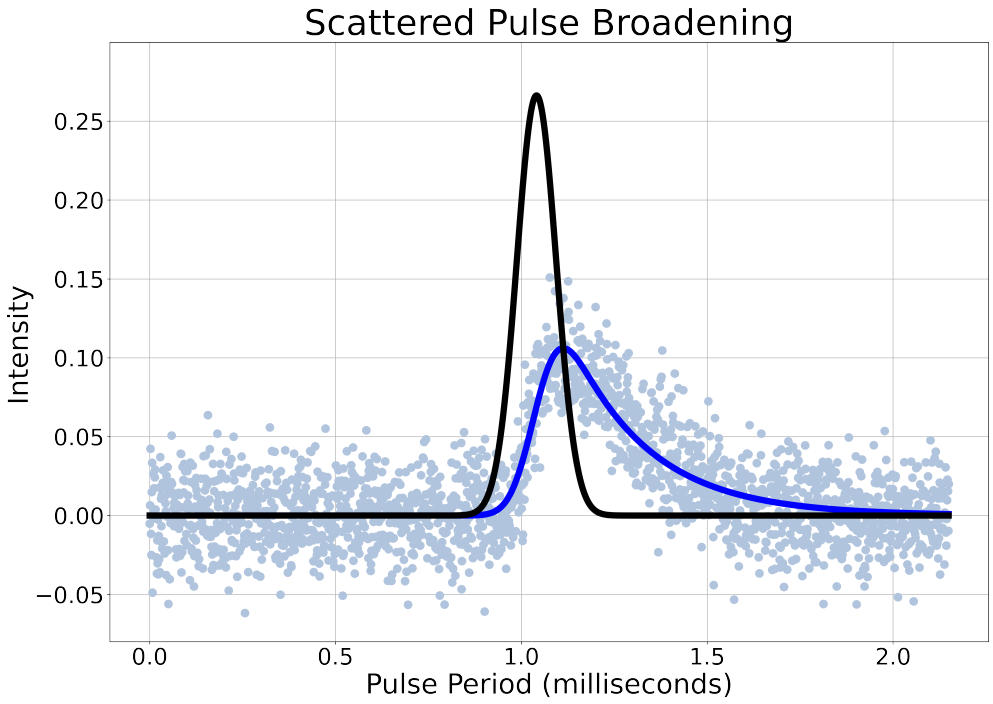


Figure 1: This plot compares the pulse profile of J1903+0327 at 1200 MHz on Mean Julian Date 57124 to a theoretical Gaussian, not convolved, with the same Gaussian amplitude, center, and width parameters. The black curve is the comparative Gaussian, and the dark blue line is the convolved line of best fit for the data in light blue. Note the evident pulse broadening exponential tail, characteristic of scattering.

$$I\left(t|A,\mu,\sigma\right) = A\exp\left(-\frac{1}{2}\left[\frac{t-\mu}{\sigma}\right]^2\right) \tag{1}$$

Where $A$ is the amplitude, $\mu$ is the pulse center, and $\sigma$ is the width or standard deviation.

However, as shown in Hemberger & Stinebring (2008), as a pulsar pulse experiences broadening through the ISM, its shape is convolved into a Gaussian plus a decaying exponential with coefficient $\tau$. This exponential is modeled with $\Theta$ as the Heaviside step function shown below.

$$h(t) = \frac{1}{\tau}\exp\left(-\frac{t}{\tau}\right)\Theta\left(t\right) \tag{2}$$

$$\Theta(t) = \begin{cases} 0 & t \leq 0 \\ 1 & t > 0 \end{cases} \tag{3}$$

The model of convolution for two functions, $I$ and $h$, is as shown (Boas, 2006, equation 10.7).

$$p(t) = I(t) * h(t) = (I * h)(t) = \int_{-\infty}^{\infty} I(u)\, h(t-u)\, du \tag{4}$$

Upon convolution, the final equation for the scattered pulse contains an error function $\Phi$, considering Gaussian integration.

$$p(t|A, \mu, \sigma, \tau) = \frac{A\sigma}{\tau}\sqrt{\frac{\pi}{2}} \exp\left(-\frac{t-\mu}{\tau}\right)\left\{1 + \Phi\left(\frac{t-(\mu+\sigma^2/\tau)}{\sigma\sqrt{2}}\right)\right\} \tag{5}$$

This is the final equation of the scattered pulse shape for fitting scattered pulsar pulses in our process.

### 4.2 Accounting for the Finite Scintle Effect

To accurately estimate for error on $\tau$, scintillation is accounted for. Broadening delays the pulse by $\tau$ itself; $\tau$ is a time delay (Hemberger & Stinebring, 2008). The finite scintle effect is used to account for errors in times of arrival, which relates to this scattering effect as a direct error on $\tau$, so the application of this error is included in our processing.

Scintillation is demonstrated by a pulsar's dynamic spectrum, a 2D surface conveying the pulsar's varying brightness over time and frequency. The error caused by the finite scintle effect relates to the number of scintles, or brightness maxima, and $\tau$ itself.

$$\sigma_{fse} = \frac{\tau}{\sqrt{N_{scintles}}} \tag{6}$$

Where $\tau$ is the measure of scattering shown previously, $N_{scintles}$ is the number of scintles or brightness maxima, and $\sigma_{fse}$ is the error on the time of arrival as caused by the finite scintle effect (Cordes & Shannon, 2010, equation 23). $N_{scintles}$ is reliant on the scintillation timescale of the pulsar, $\Delta t_d$, and frequency scale, $\Delta v_d$, because scintillation spans over time and frequency. Additionally, due to degrees of freedom, there cannot be less than one scintle in an observation (Cordes & Chernoff, 1997, appendix B).

$$N_{scintles} \approx \left(1 + \eta_t \frac{T}{\Delta t_d}\right)\left(1 + \eta_\nu \frac{B}{\Delta \nu_d}\right) \tag{7}$$

Where $\eta_t$ and $\eta_\nu$ are filling factors set to 0.2 (Cordes et al., 1990; Cordes, 1986; Cordes & Chernoff, 1997), $T$ is the observation duration, and $B$ is the observation bandwidth range. For this approximation, $\Delta \nu_d$ is calculated using the "uncertainty" relation.

$$\Delta\nu_d = \frac{C_1}{2\pi\tau_d} \tag{8}$$

$C_1$ is taken to be 1.16 for uniform scattering media (Cordes & Rickett, 1998, table 2). To calculate $\Delta t_d$, a relation to the perpendicular velocity of the pulsar is used (Cordes & Rickett, 1998, equation 13).

$$V = 2.53 \times 10^4 \text{ km/sec} \left( \frac{\sqrt{D\Delta\nu_d}}{\nu\Delta t_d} \right) \tag{9}$$

$V$ is the perpendicular velocity of the pulsar, which is estimated relying on the proper motion of the pulsar and our distance to it, taken to be 18.9 ± 10.6 km/sec as given in the NANOGrav 12.5-year data set. 18.9 km/sec is used in calculations (Alam et al., 2021). $D$ is the distance in units of kiloparsecs, 0.64 ± 0.35 kpc, with 0.64 kpc used in our calculations (Alam et al., 2021). Finally, for $\Delta t_d$ to be in units of seconds, $\nu$ is the frequency in GHz and $\Delta v_d$ is in MHz.

The count of scintles and $\sigma_{fse}$ are calculated for and incorporated into the error on $\tau$ as shown in Section 5.

### 4.3 Frequency Dependent Scattering

Scattering is exponentially related to frequency. In order to solve for the best fit of $\beta$ from $\tau$ at varying frequencies, we scale both by $\log_{10}$ and identify the slope of their relationship.

$$\tau_d = \tau_0 \left( \frac{\nu_d}{\nu_0} \right)^{\beta} \tag{10}$$

$\tau_0$ is the scattering measure at reference frequency $\nu_0$, $\tau_d$ is the scattering measure at frequency $\nu_d$, and $\beta$ is accepted as -4.4 for a characteristic Kolmogorov medium (Rickett, 1990). In this calculation, we use a reference frequency of 1 GHz.

### 4.4 Maximum Likelihood Analysis to fit $\beta$

In fitting $\tau$ as a function of frequency, we used the $\chi^2$ statistic for the $\log_{10}$-scaled, linear relationship, looping through 1500 slope and y-intercept test values.

$$\chi^2 = \sum \left[ \frac{\log_{10}(\tau_d) - \left( m \log_{10}\left(\frac{\nu_d}{\nu_0}\right) + b \right)}{\sigma_{total}} \right]^2 \tag{11}$$

$\tau_d$ is the fitted measure of scattering at frequency $\nu_d$, $\nu_0$ is the reference frequency (1 GHz), $m$ and $b$ are the test values for the slope and y-intercept, respectively, and $\sigma_{total}$ is the total error on the measured $\tau$ at this frequency. Here, in log space, the y-intercept is also equivalent to $\log_{10}(\tau_0)$. Analysis develops a 2-D surface, with axes of the parameter test values, and the absolute minimum indicates the least amount of error and the best-fit parameters for the linear relationship.

# 5 Processes

In modeling these convolved Gaussian pulses, the significance is an understanding of $\tau$, the measure of scattering, and its relationship to frequency over time. Using PyPulse, we analyzed J1903+0327 data from the 12.5-year data set. We calculated $\tau$ by fitting these pulse profiles to the convolved Gaussian and exponential shape given in Equation 5.

Coding Process:

1. Using the calibrated, time-averaged .ffz files from the NANOGrav 12.5-year data set, break up the pulse intensities of each epoch into their composing frequency channels. Analyze each frequency channel independently.
2. Define the convolved fitting function (Equation 5).
3. Define the initial fit guess parameters. scipy.optimize.leastsq() robustly calculates the fit, even with relatively weak parameter approximations.
4. Using scipy.optimize.leastsq() run the fitting function given the guess parameters for the data at each frequency, recording the returned parameters and covariance matrix error data.
5. Calculate the error from the finite scintle effect at this specific frequency and epoch as shown in §4.2.
6. Calculate the total error by adding the properly adjusted fitting error on tau to the finite scintle effect error in quadrature.
7. Repeat this for each frequency channel in the epoch, calculating $\tau$ values with error.
8. Convert this scattering-frequency relationship to log scales, accounting for the change in error via propagation of uncertainty.

$$f = \log_{10}(\tau) \tag{12}$$

$$\sigma_f \approx \left| \frac{\sigma_\tau}{\tau \log_e(10)} \right| \tag{13}$$

9. Loop through different values of $\beta$ and $\tau_0$ for the $\log_{10}$-scaled relationship of $\tau$ and $\nu$, and calculate the $\chi^2$ values for each. Find the maximum likelihood, which effectively denotes the parameters of best fit.

10. Remove outliers from this fit based on visual evaluation, with consideration of error bars, and recalculate the linear best fit as necessary.

11. Repeat this process for all epochs, finally gathering the timescale of $\tau$, or scattering.

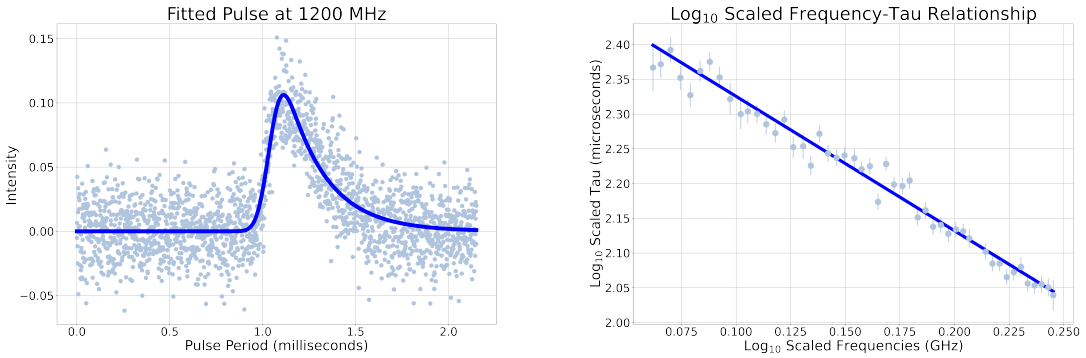


Figure 2: Left: The coding process outcome for steps 2-4. The fitted Gaussian-exponential pulse is calculated from pulse profile data at the frequency of 1200 MHz. Right: The coding process outcome for steps 7-10. The fitted line for the fitted, $\log_{10}$-scaled $\tau$ values for each $\log_{10}$-scaled frequency channel is calculated.

One advantage of this analysis is that it fits for all pulse shape parameters, including the pulse center; there is a separation from dispersion because the pulse shape itself is considered, not where it is centered.

## 6 Results

For pulsar J1903+0327, our results show a weighted average frequency scaling relationship of $\beta = -2.7 \pm 0.5$ for scattering. These $\beta$ values raise multiple dilemmas. First, the average $\beta$ value here differs significantly from the accepted Kolmogorov value of -4.4. Other observations to note are the changes in these values over time. The error bars on $\beta$ are too small to ignore these variations in scattering.

One possible explanation for these $\beta$ variations is the influence of a scattering medium with variable strength transverse to the line of sight.

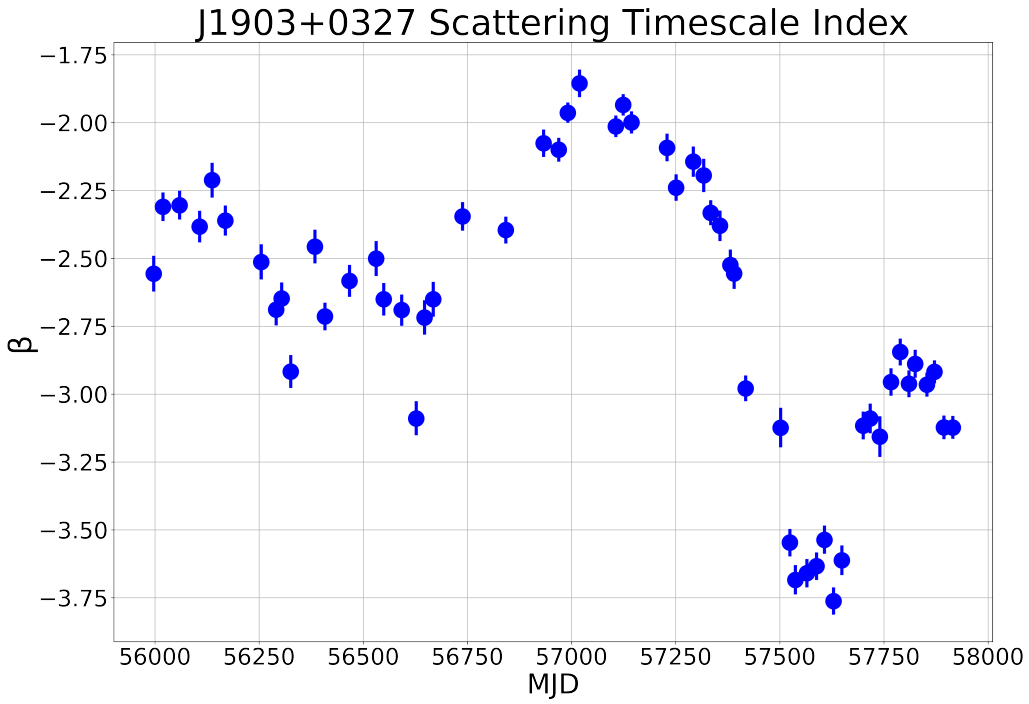


Figure 3: Shown above are the values of $\beta$ for the exponential relationship of frequency and scattering per epoch over time.

# 7 New Frontiers

## 7.1 Refractive Scintillation

Refractive scintillation could play a part in the variation of $\beta$ given that refraction relates to frequency but differs in frequency dependence from diffractive scintillation. We estimated the refractive timescales of J1903+0327 with the following approximation from Stinebring & Condon (1990).

$$T_r \approx \frac{4}{\pi}\left(\frac{\nu T_d}{\Delta\nu_d}\right) \tag{14}$$

Refractive timescales vary based on the frequency of the pulse profile in question, and for pulsar J1903+0327, these refractive timescales range from roughly 1 to 2 years. This is significant because the variations in $\beta$ occur approximately at this timescale. Further investigation is warranted.

### 7.2 Parameter Covariances

In order to best explain the dramatic variation in the indices of the frequency-scattering relationship, it is important to understand covariance between the convolved Gaussian-exponential fit parameters. To ensure that the frequency-dependent variations observed in $\tau$ are not caused by frequency-dependent variations in width, width timescales were calculated in the same manner as scattering. We call the indices of this frequency-width relationship $\gamma$. However, $\gamma$ and $\beta$ values have a moderately weak correlation coefficient of -0.44. The Markov Chain Monte Carlo simulation is one statistical method of increased robustness that we are currently implementing. The average correlation coefficient with respect to width and $\tau$ chain samples across all channels and epochs is $-0.5 \pm 0.1$; however, these correlation coefficients are relatively consistent over time and do not evidently exhibit trends that impact our results. Further investigation into covariances is warranted.

## Acknowledgments

We graciously acknowledge support received from NSF AAG award number 2009468, and NSF Physics Frontiers Center award numbers 1430284 and 2020265, which support the NANOGrav project.

## References

Alam, M. F., Arzoumanian, Z., Baker, P. T., et al. 2021, *ApJS*, 252, 4. doi:10.3847/1538-4365/abc6a0

Champion, D. J., Ransom, S. M., Lazarus, P., et al. 2008, Science, 320, 1309. doi:10.1126/science.1157580

Cordes, J. M. 1986, *ApJ*, 311, 183. doi:10.1086/164764

Cordes, J., McLaughlin, M. A., & Nanograv Collaboration 2019, *BAAS*, 51, 447

Cordes, J. M., Wolszczan, A., Dewey, R. J., et al. 1990, *ApJ*, 349, 245. doi:10.1086/168310

Cordes, J. M. & Chernoff, David. F. 1997, *ApJ*, 482, 971. doi:10.1086/304179

Cordes, J. M. & Rickett, B. J. 1998, *ApJ*, 507, 846. doi:10.1086/306358

Cordes, J. M. & Shannon, R. M. 2010, arXiv:1010.3785

Hemberger, D. A. & Stinebring, D. R. 2008, *ApJL*, 674, L37. doi:10.1086/528985

Mary L. Boas. Mathematical methods in the physical sciences; 3rd ed. 2006.

Rickett, B. J. 1990, *ARAA*, 28, 561. doi:10.1146/annurev.aa.28.090190.003021

Stinebring, D. R. & Condon, J. J. 1990, *ApJ*, 352, 207. doi:10.1086/168528